Venegas, M.; Vega, M.; García-Hernando, N.; Ruiz-Rivas, U. (2016). A simple model to predict the performance of a H2O–LiBr absorber operating with a microporous membrane. *Energy*, v. 96, pp. 383-396. DOI: 10.1016/j.energy.2015.12.059

A simple model to predict the performance of a H_2O LiBr absorber operating with a microporous membrane

M. Venegas [a, b, c, *], M. de Vega [a, c], N. García-Hernando [a, c], U. Ruiz-Rivas [a, b]

[a] ISE Research Group, Department of Thermal and Fluids Engineering, Universidad Carlos III de Madrid, Avda. Universidad 30, 28911 Leganés, Madrid, Spain
[b] GTADS Research Group, Department of Thermal and Fluids Engineering, Universidad Carlos III de Madrid, Avda. Universidad 30, 28911 Leganés, Madrid, Spain
[c] Associated Research Unit CSIC-Universidad Carlos III de Madrid, Spain

Keywords:
Absorption refrigeration
Membranes
Absorber
Water-lithium bromide
Rectangular microchannels

A B S T R A C T

A microporous membrane is used in combination with rectangular microchannels in the absorber of an absorption chiller with the aim of reducing the size of this cooling technology. The simulation of the heat and mass transfer between the solution and the vapour phase in a H_2O LiBr absorber using porous fibres is considered. Heat and mass transfer processes are modelled by means of selected correlations and data gathered from the open literature. This new model is applied for the simulation of the absorber under typical operating conditions of absorption cooling chillers. Absorption rate, heat and mass transfer co efficients, solution concentration, temperatures of the working fluids and pressure potential along the absorption channels are calculated. For the case considered in this study, the absorber channels are of 5 cm length, offering a maximum ratio between cooling capacity of the chiller and absorber volume of 1090 kW/m^3. This ratio is higher than twice the usual values found in falling film absorbers using conventional circular tubes. The mean absolute error between the model results and the experimental data gathered from the open literature is 8.5%, showing the capability of the model to predict the per formance of membrane based absorbers.

1. Introduction

Absorption chillers and heat pumps have received growing attention over the last few decades since they allow the use of low grade heat to produce a cooling effect, with no (or minimal) me chanical power consumption. For example, absorption cooling machines can use waste heat or excess heat from solar collectors in the form of hot water for cooling purposes. In buildings, they could help to optimize the solar thermal energy in the summer period reducing the electricity consumption peak due to air conditioning. Nevertheless, their use is limited, compared to mechanical refrig eration systems, because they are generally larger in size, limiting to a great extend their use in low and medium power applications. For instance, a typical value for the volume to refrigeration power ratio in single effect absorption chillers is in the order of 0.04 m^3/kW (without considering the volume occupied by the cooling system) for refrigeration capacities between 10 and 30 kW, whereas mechanical compressor systems can have a ratio equal to 0.02 m^3/kW for the same range of refrigeration capacities (García Hernando et al. [1]).

The absorber is one of the most performance limiting and vol ume demanding components of absorption systems. In the absorber, the concentrated liquid solution absorbs the refrigerant vapour that comes from the evaporator. The main challenge in designing and operating these devices is to maximize the mass transfer rate by getting as much interfacial area as possible. Several configurations for the liquid and vapour streams in the absorber have been proposed in order to increase the heat and mass transfer in the liquid solution: falling films, bubbles, sprays and droplets, liquid jets and sheets, etc. Nevertheless, all of them present rela tively low heat and mass transfer coefficients and lead to large, heavy and rigid heat exchangers. Other authors proposed the use of Plate Heat Exchangers in the absorber or the desorber, in order to increase the cooling capacity to volume ratio in absorption systems (Venegas et al. [2], de Vega et al. [3]). At present, a promising new technology is under study, consisting in the use of membrane contactors in microchannel heat exchangers.

* Corresponding author. ISE Research Group, Department of Thermal and Fluids Engineering, Universidad Carlos III de Madrid, Avda. Universidad 30, 28911 Leganés, Madrid, Spain. Tel.: +34 916248776; fax: +34 916249430.
E-mail address: mvenegas@ing.uc3m.es (M. Venegas).

Nomenclature

A	area (m^2)
b	molality (mole kg^{-1}_{water})
c_B	Boltzmann constant (J K^{-1})
C_p	specific heat (kJ kg^{-1} K^{-1})
dz	discretization length (m)
D	diffusion coefficient (m^{-2} s^{-1})
D_h	hydraulic diameter (m)
d_p	membrane pore diameter (m)
e	height or thickness (m)
h	convective heat transfer coefficient (W m^{-2} K^{-1})
i	specific enthalpy (kJ kg^{-1})
J	absorption rate (kg m^{-2} s^{-1})
k	thermal conductivity (W K^{-1} m^{-1})
K	mass transfer coefficient (kg Pa^{-1} m^{-2} s^{-1})
Kn	Knudsen number, $Kn \quad \lambda/d_p$
l	width (m)
L	total length of channels (m)
$\dot{m}$	mass flow rate (kg s^{-1})
M	molecular weight (kg $mole^{-1}$)
N	number of channels
Nu	Nusselt number, $Nu \quad hD_h/k$
P	pressure (Pa)
Pr	Prandtl number, $Pr \quad \mu C_p/k$
q	thermal power (W)
R	mass transfer resistance (kg^{-1} Pa m s)
Re	Reynolds number, $Re \quad uD_h\rho/\mu$
R_u	universal gases constant (J $mole^{-1}$ K^{-1})
Sc	Schmidt number, $Sc \quad \mu/\rho D$
Sh	Sherwood number, $Sh \quad KD_h/D$
T	temperature (°C)
u	velocity (m s^{-1})
U	global heat transfer coefficient (W m^{-2} K^{-1})
x	lithium bromide mass fraction (kg_{LiBr} kg_s^{-1})
z	length (m)

Greek symbols

α	channel aspect ratio, $\alpha \quad l/e$.
ΔT	temperature difference (°C)
ε	porosity
λ	mean free path (m)
μ	viscosity (Pa s)
Ξ	Ackermann factor
ρ	density (kg m^{-3})
σ	molecular collision diameter (Å)
τ	tortuosity
Φ	heat transfer rate factor

Subscripts

cw	cooling water
l	liquid
m	membrane
ov	overall
s	solution
sat	saturation
th	thermal
T	total
v	vapour
va	vapour absorbed
w	wall

Membrane based absorbers use a microporous polymeric membrane at the solution refrigerant vapour interface. In the membrane, many small diameter pores avoid mixing between vapour and solution, while allow the gas and solution to be in contact. Surface tension prevents the solution from entering the holes, while the gas diffuses to the solution surface through the pores. In the absorber, the gaseous fluid (typically ammonia or water) passes the membrane and is absorbed by the solution (NH_3–H_2O or H_2O–LiBr respectively) flowing inside constrained flow passages. The vapour pressure difference through the membrane is the driving force for mass transfer. If the partial pressure of the vapour inside the solution is less than the vapour pressure, it is absorbed at the interface between solution and vapour. Compared with conventional absorption devices, there are several advantages of using microporous fibre modules for vapour absorption. These include larger interfacial area per unit volume, independent control of vapour and liquid flow rates, easier scale up, modular design and compactness.

Concerning ammonia water systems, Chen et al. [4] theoretically modelled and simulated an absorber using hollow fibre membranes and compared the results to a plate heat exchanger absorber of falling film type. In their model, they considered the ammonia–water concentration across this microporous membrane as the driving potential for mass transfer. The comparisons of the heat and mass transfer coefficients of both devices revealed that the vast interfacial area of the membrane solution is the major reason for achieving higher absorption performance. Schaal et al. [5] experimentally investigated a NH_3–H_2O absorber using a hollow fibre hydrophobic microporous membrane in order to get basic design data. Ghiasi et al. [6] conducted experimental research to investigate the absorption of ammonia vapour into the solution, with the main objective of optimizing the absorber within the whole refrigeration system to optimize the system performance.

In H_2O–LiBr applications, Isfahani and Moghaddam [7] tested an absorber using a superhydrophobic nanofibrous membrane with nominal pore size of 1 micron and 80% porosity. They obtained an absorption rate of about 0.006 kg/m^2s, using channels of 100 micron thickness and a flow velocity of 5 mm/s. Isfahani et al. [8] presented a study on the efficacy of highly porous nanofibrous membranes for application in membrane based absorbers and desorbers. Permeability studies showed that membranes with a pore size greater than about 1 micron are valid for their application in absorbers. Ali and Schwerdt [9] experimentally and analytically investigated the characteristics and properties of commercially available microporous hydrophobic membranes. They evaluated some factors that influence the water vapour (refrigerant) mass transfer flux into a thin lithium bromide–water solution confined in narrow channels. Yu et al. [10] numerically investigated the performance of a membrane based absorber using the H_2O–LiBr solution. They showed that several folds enhancement in the absorption rate can be achieved with respect to conventional absorbers. When the film thickness was reduced from 150 to 50 microns, the absorption rate increased 3 fold. When the solution velocity was quadrupled, the average absorption rate increased 50%. Bigham et al. [11] showed that mass transport in the microfilm solution could be improved by the implementation of micro scale features on the flow channel surface. Recently a review of membrane contactors applied in absorption refrigeration systems has been done by Asfand and Bourouis [12].

According to the literature review, in order to optimize the heat and mass process to minimize the absorber volume, detailed studies about the role of the relevant parameters in the absorption process are still necessary. In the present investigation, the water lithium bromide solution has been selected. This working pair is adequate for evaporation temperatures higher than 0 °C, and it is the most common solution used for air conditioning applications, according to Henning [13]. Moreover, these systems can be fed with low temperature heat. The present study focuses therefore in the absorber modelling of the heat and mass transfer in the micropo rous membrane coupled with the cooling of the solution in a H_2O—LiBr absorber.

2. Modelling of the absorption process

The absorber configuration used in the present study is shown in Figs. 1 and 2. It is a plate and frame membrane module with geometrical data and operating variables described in Table 1. The module contains a vapour channel, separated from the solution by an adjacent microporous membrane. The solution is confined in microchannels. The upper side of these channels is the hydrophobic membrane. A metal wall separates the solution channels from the cooling water channels. Water lithium bromide solution is used.

In order to simplify the problem, the following assumptions are considered:

- The system operates under steady state conditions.
- The solution, cooling water and refrigerant vapour completely fill their respective channels: no incondensable gases are pre sent and vapour absorption takes place instantaneously.
- The plate and frame membrane module is adiabatic with respect to its surroundings.
- An equilibrium state exists at the vapour/liquid interface.
- Solution, cooling water and vapour are well mixed in each dif ferential volume. Homogeneous temperature and concentration are considered in all points within each respective control volume.
- The heat and mass transfer are one dimensional.
- Pressure is constant along the channels. As a result, the solution equilibrium concentration is only a function of the solution temperature.

As a novelty regarding membrane based absorbers, the heat and mass transfer models consider that temperature and/or concen tration are changing along both thermal entrance and fully developed flow regions. Additionally, the influence of mass transfer on heat transfer, which has not been included before in similar investigations, is taken into account.

In the following Sections (2.1 and 2.2), the general equations defining the heat and mass transfer models are presented. In Sec tion (2.3), the correlations and data gathered from the open liter ature, required to implement the heat and mass transfer models, are grouped together and discussed.

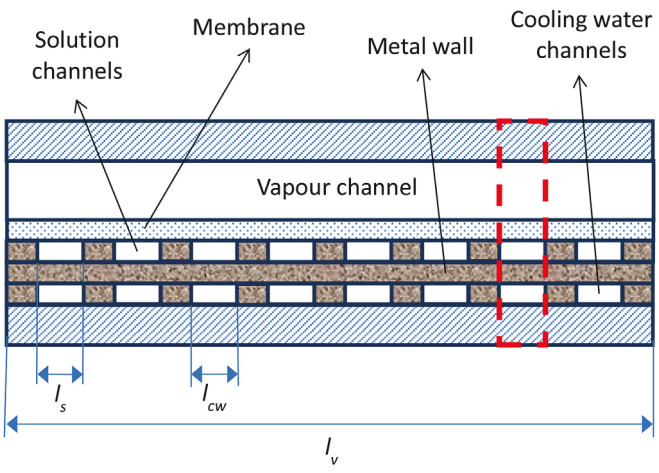

Fig. 1. Cross section of the plate and frame membrane-based absorber.

2.1. Mass transfer model

The vapour mass flux through the membrane is calculated tak ing into account the conditions in the bulk water vapour and bulk aqueous solution streams. For the differential element j, the mass flow rate is:

$$\dot{m}_{va}^{j} \quad J^{j} \cdot A \tag{1}$$

where A is the heat and mass transfer area:

$$A \quad l_s \cdot dz \tag{2}$$

and J is the absorption rate:

$$J^{j} \quad \frac{P_v \quad P_s^{j}}{R_{ov}^{j}} \tag{3}$$

P_v and P_s are the bulk vapour pressure and the water vapour partial pressure corresponding to the bulk solution concentration (x) and temperature (T_s), according to Ali [14]. The overall mass transfer resistance between the bulk water vapour and bulk aqueous solution (R_{ov}) includes the resistance to diffusion through the aqueous solution boundary layer (R_s) and the resistance to diffusion of water vapour through the membrane active layer (R_m). Both resistances act in series:

$$R_{ov}^{j} \quad R_s^{j} + R_m^{j} \tag{4}$$

Equations used to calculate R_s^j and R_m^j are described in Section 2.3.1.

Mass rate balances for the solution and the water vapour give the mass flow rates in the differential element $j + 1$:

$$\dot{m}_s^{j+1} \quad \dot{m}_s^{j} + \dot{m}_{va}^{j} \tag{5}$$

$$\dot{m}_v^{j+1} \quad \dot{m}_v^{j} \quad \dot{m}_{va}^{j} \tag{6}$$

Mass fraction of lithium bromide in the solution is calculated from:

$$x^{j+1} \quad x^{j} \frac{\dot{m}_s^{j}}{\dot{m}_s^{j+1}} \tag{7}$$

2.2. Heat transfer model

The energy rate balance applied to the differential element j is written as:

$$(\dot{m}_{va} i_{lv})^{j} \quad q_s^{j} + q_v^{j} + q_{cw}^{j} \tag{8}$$

Left term in Eq. (8) corresponds to the thermal power released during absorption of the vapour flow rate $\dot{m}_{va}$ into the solution. Right terms are related to the heat transferred to the solution, vapour and cooling water respectively. These can be calculated, for parallel flow, as:

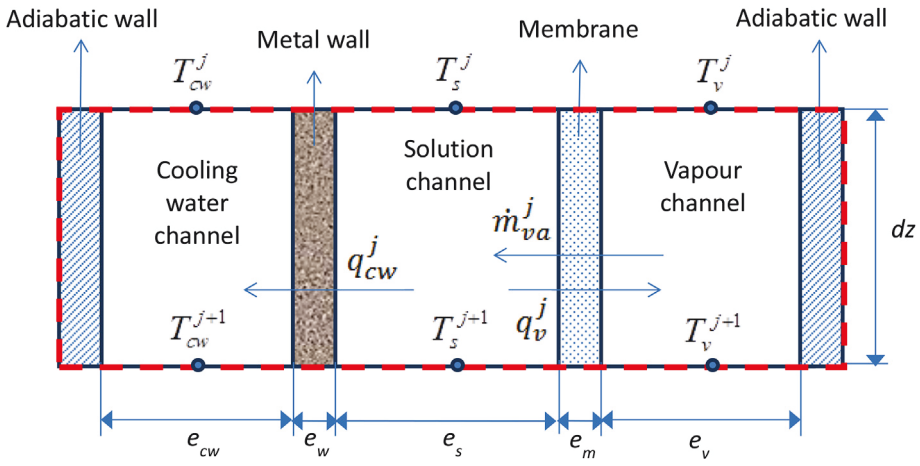

Fig. 2. Differential element of the absorber.

Table 1
Data considered for the simulation, corresponding to the schemes of the absorber represented in Figs. 1 and 2.

Parameter	Value
Cooling water inlet temperature, T_{cw} (°C)	27
Solution inlet temperature, T_s (°C)	32
Vapour inlet temperature, T_v (°C)	7
Membrane pore diameter, d_p (μm)	1
Vapour pressure, P_v (kPa)	1
Porosity, ε	0.8
Cooling water channel height, e_{cw} (mm)	0.15
Metal wall thickness, e_w (mm)	2.7
Solution channel height, e_s (mm)	0.15
Membrane thickness, e_m (μm)	60
Vapour channel height, e_v (mm)	5
Solution channel centre-to-centre distance, w_s (mm)	1.6
Cooling water channel centre-to-centre distance, w_{cw} (mm)	1.6
Cooling water channel width, l_{cw} (mm)	1.5
Solution channel width, l_s (mm)	1.5
Vapour channel width, l_v (mm)	20.9
Number of solution channels, N_s	13
Number of cooling water channels, N_{cw}	13
Length of channels, L (mm)	50
Discretization length, dz (mm)	0.22
Total solution mass flow rate at the inlet, $m_{s,T}$ (g/s)	1
Total cooling water mass flow rate, $m_{cw,T}$ (g/s)	0.5
Vapour mass flow rate at the inlet, m_v (g/s)	0.0032
LiBr mass fraction at the inlet, x	0.6

$$q_s^j \quad (\dot{m}\cdot i)_s^{j+1} \quad (\dot{m}\cdot i)_s^j \tag{9}$$

$$q_v^j \quad (\dot{m}\cdot i)_v^{j+1} \quad (\dot{m}\cdot i)_v^j \tag{10}$$

$$q_{cw}^j \quad \dot{m}_{cw}\left(i_{cw}^{j+1} \quad i_{cw}^j\right) \quad \dot{m}_{cw}Cp_{cw}^j\left(T_{cw}^{j+1} \quad T_{cw}^j\right) \tag{11}$$

Last term of Eq. (11) considers that cooling water is an incom pressible liquid with constant specific heat.

The present model also considers that heat is transferred from the bulk solution channel (where absorption takes place) to both cooling water and vapour channels. In this case the following re lations are also valid:

$$q_{cw}^j \quad U_{s\_cw}^j A\left(T_s^j \quad T_{cw}^j\right) \tag{12}$$

$$q_v^j \quad U_{s\_v}^j A\left(T_s^j \quad T_v^j\right) \tag{13}$$

The global heat transfer coefficients in Eqs. (12) and (13) are calculated as:

$$\frac{1}{U_{s\_cw}^j} \quad \frac{1}{h_{cw}^j} + \frac{e_w}{k_w^j} + \frac{1}{h_{s,cw*}^j} \tag{14}$$

$$\frac{1}{U_{s\_v}^j} \quad \frac{1}{h_v^j} + \frac{e_m}{k_{m,ave}^j} + \frac{1}{h_{s,v*}^j} \tag{15}$$

Equations and data used to calculate the local convection heat transfer coefficients and the thermal conductivities are described in Section 2.3.2.

The concentration and temperatures along the channels cannot be explicitly determined from Eqs. (1)–(15). For this reason, the above set of equations should be solved iteratively. They have been compiled in a computer code developed by the authors using En gineering Equation Solver software, EES™ (Klein [15]). Fig. 3 shows the flowchart used for implementing the heat and mass transfer models.

Main advantages of the present heat and mass transfer models include:

- Less time consuming than detailed numerical codes. Calculation time is less than 30 s.
- Simplicity of the model allows its implementation using any programming language. In this case EES™ has been selected, because of its high accurate thermodynamic and transport property database that can be used with the equation solving capability [15].
- No hypothesis about temperature distribution along the cooling water channel is required.
- Heat transfer to vapour channel is not neglected.

2.3. Selection of correlations and data

In order to implement the heat and mass transfer models developed in the previous sections, data and correlations available in the open literature were carefully revised and appropriated ones selected, taking into account their adequacy to the simulated conditions.

Thermodynamic properties of water lithium bromide solution have been calculated using EES™, which uses correlations devel oped by Patek and Klomfar [16] for all properties, except for vis cosity and thermal conductivity. In this case, EES uses correlations provided by DiGuilio et al. [17]. Properties of water are also

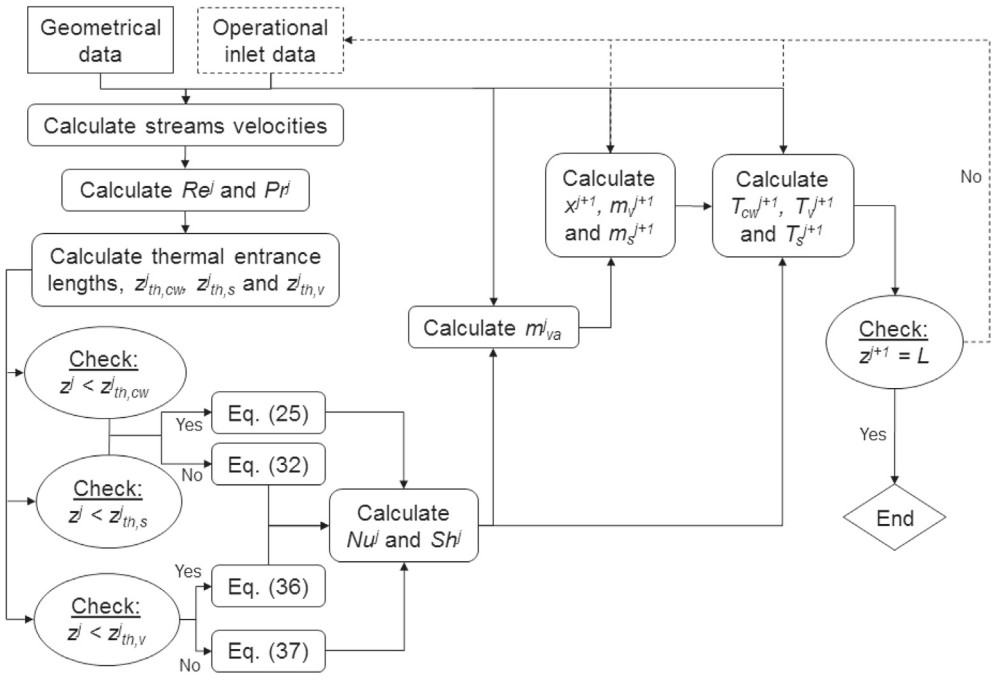

Fig. 3. Flowchart for simulating the heat and mass transfer process along the absorption channel.

calculated using EES: the correlation of Harr et al. [18] for the thermodynamic properties and transport ones using equations of the Electrical Research Association [19]. Thermal conductivity of the metal wall was assumed to be 10 W/mK. This is a typical value for corrosion resistant metals and alloys (Chawla and Gupta [20]).

2.3.1. Mass transfer

To calculate the mass flux through the membrane, the flow regime must first be determined. Knudsen number (Kn) is used to evaluate the transport of water vapour across the membrane: when Kn is less than 0.01, collisions between gas molecules dominate and viscous flow occurs, resulting in rapid convective transport. When Kn is equal or larger than 10, collisions between molecules and pore walls are dominant, and the gas transport takes place via Knudsen flow (free molecular regime). Transitional regime exists if $0.01 < Kn < 10$. Knudsen number is defined as:

$$Kn \quad \lambda / d_p \tag{16}$$

where λ is the mean free path of the water vapour (distance between molecular collisions) and d_p is the membrane pore diameter. In this work, the mean free path is calculated using the equation given by Redhead et al. [21]:

$$\lambda \quad \frac{c_B T_m}{\sqrt{2}\pi\sigma^2 P_m} \tag{17}$$

where c_B is the Boltzmann constant ($1.38 \cdot 10^{-23}$ J/K), T_m is the absolute temperature (K), σ is the molecular collision diameter (2.641 Å for water vapour) and P_m is the mean total pressure within the membrane pores (Pa).

For the current study, the calculated Knudsen number value changes very slightly around 13.6. Consequently, free molecular flow occurs through the membrane along the whole absorber.

According to the Dusty Gas model, described by Mason and Malinauskas [22] and applied by Yu et al. [10] to a similar problem, and taking into account that free molecular flow is present in the membrane, the mass transfer coefficient through the membrane K_m can be estimated as:

$$K_m \quad \frac{M}{e_m} \quad \frac{D_e^K}{R_u T_m} \quad 1/R_m \tag{18}$$

where the diffusion term can be evaluated as:

$$D_e^K \quad \frac{\varepsilon d_p}{3\tau} \left(\frac{8 R_u T_m}{\pi M} \right)^{0.5} \tag{19}$$

In Eq. (18), e_m is the membrane thickness. In Eqs. (18) and (19), M is the molecular weight of water and R_u is the universal gases constant. In Eq. (19), ε and τ are the porosity and tortuosity of the membrane, respectively. Tortuosity of the membrane is calculated as a function of the membrane porosity, according to Iversen et al. [23]:

$$\tau \quad \frac{(2 \quad \varepsilon)^2}{\varepsilon} \tag{20}$$

Resistance to mass transfer inside the bulk solution R_s can be calculated according to Ali and Schwerdt [9], as:

$$R_s \quad \frac{P_{sat}}{\rho_{water} K_s} \tag{21}$$

where P_{sat} is the saturated water pressure corresponding to the bulk solution temperature, ρ_{water} is the liquid water density and K_s is the mass transfer coefficient between the solution–vapour interface and the bulk aqueous solution. A suitable correlation for mass transfer in microchannels has not been found in the open literature. For this reason, the mass transfer coefficient of the solution is calculated using mass and heat transfer analogy, using correlations of Lee and Garimella [24] for the thermal entrance region and Shah and London [25] for the fully developed flow. These correlations are described in the next section.

The use of Sherwood and Schmidt dimensionless numbers to obtain the solution mass transfer coefficient requires knowledge of the diffusion coefficient. In this study, it was corrected by temperature using the equation described by Mittermaier et al. [26]:

$$D \quad D(25\,^{\circ}\mathrm{C})\frac{T+273.15}{298.15}\frac{\mu(25\,^{\circ}\mathrm{C})}{\mu(T)} \tag{22}$$

where the diffusion coefficient at 25 °C is calculated as:

$$D(25\,^{\circ}\mathrm{C}) \quad \left(1.3528+0.19881b \quad 0.036382b^2+0.0020299b^3 \quad 0.000039375b^4\right)10^{-9} \tag{23}$$

Parameter b in Eq. (23) is the molality, obtained from:

$$b \quad \frac{x}{M_{\mathrm{LiBr}}(1 \quad x)} \tag{24}$$

M_{LiBr} is the molecular weight of the lithium bromide.

2.3.2. Heat transfer

The convection heat transfer coefficients, in Eqs. (14) and (15), along the solution, cooling water and vapour channels, have been calculated taking into account two regions: thermal entrance re gion and fully developed flow. Correlations to be used were selected also considering the dimensions of the channels.

In the case of the solution and cooling water channels, with $D_{h,s} \quad D_{h,cw} \quad 272.7$ μm, equations of Lee and Garimella [24] for microchannels were used to estimate the length of the thermal entrance region and the convection heat transfer coefficients in this region. This correlation has the advantage, with respect to others available in the open literature, of allowing the estimation of the heat transfer coefficient as a function of the position along the channel. Also, it covers a sufficiently broad range of aspect ratios and hydraulic diameters.

$$Nu_{th} \quad \frac{1}{C_1(z^*)^{C_2}+C_3}+C_4, \quad \text{for } 1\le\alpha\le 10,\ z^*<z^*_{th} \tag{25}$$

The channel aspect ratio is $\alpha \quad l/e$. The dimensionless axial distance z^* is:

$$z^* \quad z/(RePrD_h) \tag{26}$$

The dimensionless length of the thermal entrance region is:

$$z^*_{th} \quad 1.275\cdot10^{-6}\alpha^6+4.709\cdot10^{-5}\alpha^5 \quad 6.902\cdot10^{-4}\alpha^4 + 5.014\cdot10^{-3}\alpha^3 \quad 1.769\cdot10^{-2}\alpha^2+1.845\cdot10^{-2}\alpha + 5.691\cdot10^{-2} \tag{27}$$

and:

$$C_1 \quad 3.122\cdot10^{-3}\alpha^3+2.435\cdot10^{-2}\alpha^2+2.143\cdot10^{-1}\alpha+7.325 \tag{28}$$

$$C_2 \quad 0.6412 \tag{29}$$

$$C_3 \quad 1.589\cdot10^{-4}\alpha^2 \quad 2.603\cdot10^{-3}\alpha+0.02444 \tag{30}$$

$$C_4 \quad 7.148 \quad \frac{13.28}{\alpha}+\frac{15.15}{\alpha^2} \quad \frac{5.936}{\alpha^3} \tag{31}$$

Convection heat transfer coefficients along the microchannels for the fully developed flow were obtained using the correlation developed by Shah and London [25]. This correlation is valid for rectangular channels, which is the present case:

$$Nu \quad 8.235\left(1 \quad \frac{2.0421}{\alpha}+\frac{3.0853}{\alpha^2} \quad \frac{2.4765}{\alpha^3}+\frac{1.0578}{\alpha^4} \quad \frac{0.1861}{\alpha^5}\right) \tag{32}$$

In the case of the solution channel, the effect of mass transfer on heat transfer was taken into account using a modified heat transfer coefficient. Coefficients obtained using Eqs. (25) and (32) were corrected, multiplying them by the Ackermann factor (Taylor and Krishna [27]):

$$\Xi \quad \frac{\Phi}{e^{\Phi} \quad 1} \tag{33}$$

where the heat transfer rate factor Φ is defined as:

$$\Phi \quad J\cdot Cp_v\cdot e_s/k_v \tag{34}$$

The modified convection coefficient, for heat transfer from the solution to the cooling water channel, is incremented because mass transfer is taking place in the same direction of heat transfer. In the case of heat transfer to the vapour channel the coefficient is reduced because the processes occur in opposite directions.

The vapour channel is a conventional rectangular channel with $D_{h,v} \quad 8.1$ mm. In this case, the dimensionless thermal entry length is calculated using the following correlation, derived in this research from data tabulated by Shah and London [25] for the case of simultaneously developing flow:

$$z^*_{th,v} \quad \frac{0.205}{\alpha_v^2}+\frac{0.5282}{\alpha_v}+0.0169, \ \text{with} \quad R^2 \quad 1 \tag{35}$$

Data tabulated also by Shah and London [25], for the case of constant heat flux, were used to derive the following correlation for Nu in this developing region. It is valid for the aspect ratio of the vapour channel used in the present study, $\alpha_v \quad 4$.

$$Nu_{th,v} \quad 3\cdot10^{-5}\left(z^*_v\right)^2+0.0307z^*_v+5.2901, \ \text{with} \quad R^2 \quad 0.999 \tag{36}$$

Finally, for the thermally developed flow, a correlation was also derived from data tabulated by Shah and London [25] for the case of constant heat flux:

$$Nu_v \quad \frac{0.037}{\alpha_v^2}+\frac{0.7639}{\alpha_v}+2.8036, \quad \text{for } 1 \ \le \ \alpha_v \ \le \ 10, \quad \text{with} \quad R^2 \quad 0.998 \tag{37}$$

The average thermal conductivity of the membrane, $k_{m,ave}$ in Eq. (15), is calculated using the equation given by Martínez and Rodríguez Maroto [28]:

$$k_{m,ave} \quad \varepsilon k_v+(1 \quad \varepsilon)k_m \tag{38}$$

In Eq. (38), k_v is the thermal conductivity of the vapour inside the membrane pores, while k_m is the thermal conductivity of the membrane solid material. A polytetrafluoroethylene (PTFE) mem brane has been selected, with thermal conductivity equal to 0.22 W/mK, the same used by Ali [14].

2.4. Model validation

Validation of the model has been performed comparing the absorption rate predicted with the experimental data reported by Isfahani and Moghaddam [7]. In the experimental case, the solution and cooling water channels measure 1 and 4 mm in width respectively, while two different heights for the solution channel, 0.1 and 0.16 mm, were used. The cooling water channel height was 0.4 mm. An important issue is that the correlations used in the present model remain valid in all the cases.

Figs. 4–7 show a comparison between the absorption rate predicted by the model, using the data of Isfahani and Moghaddam [7], and their experimental results. Fig. 4 shows the variation of the absorption rate as a function of the vapour pressure and the solution channels height. A similar trend is obtained in both cases. The almost parallel lines show the good prediction of the model concerning the vapour pressure increase influence: the absorption rate increases because the vapour pressure potential rises. Also, a better absorber performance is obtained in both cases for the less deep channel. This outcome coincides with simulation results presented in the next section about the influence of the solution channel aspect ratio, i.e. higher aspect ratios contribute to higher absorption ratios.

The influence of the cooling water inlet temperature on the absorption rate is represented in Fig. 5 for the two solution channel heights of the experiments. Again, the model predicts a tendency similar to the experiments in both cases. The increase in the cooling water inlet temperature reduces the driving force for heat transfer between the solution and the cooling water, leading to an increase of the solution temperature. Consequently, the solution water vapour pressure increases, which reduces the vapour pressure potential for mass transfer. As observed in Figs. 4 and 5, the difference between the simulation results and the experiments increases when the solution channel height decreases. One reason for this higher difference can be attributed to the tolerance in the channels manufacturing, 10 μm in both cases, representing up to 10% of the channel height in the case of the 100 μm channel.

The combined influence of the solution mass flow rate and the vapour pressure on the absorption ratio is shown in Fig. 6. Again, small differences exist between the experiments and the model results and similar trends are observed in all the cases. As observed,

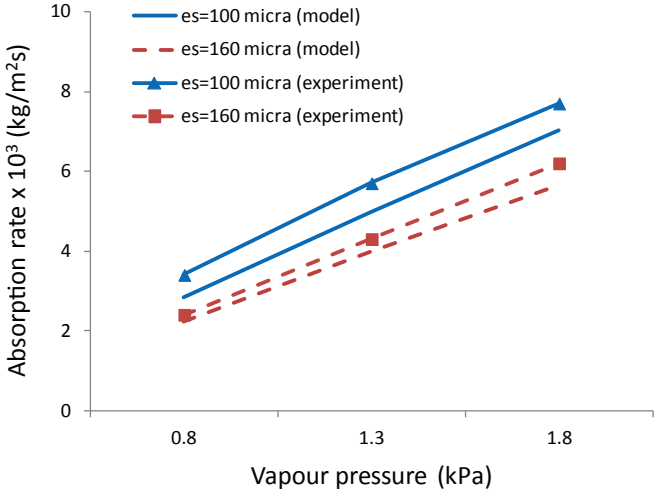

Fig. 4. Absorption rate as a function of the vapour pressure and the solution channel height (e_s). Comparison between model and experimental results of Isfahani and Moghaddam [7].

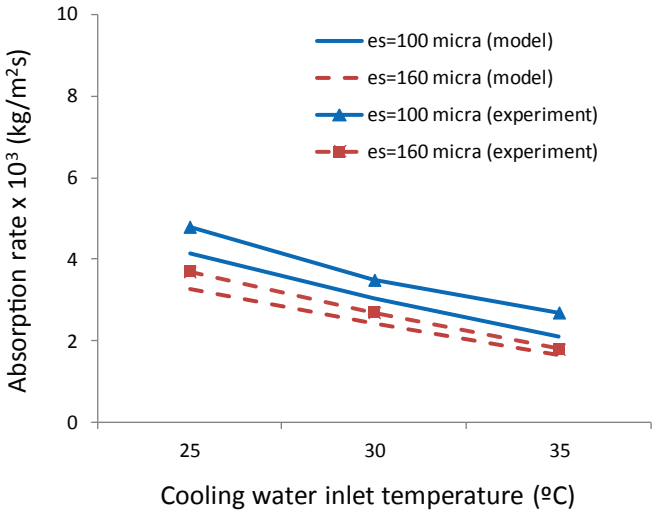

Fig. 5. Absorption rate as a function of the cooling water inlet temperature and the solution channel height (e_s). Comparison between model and experimental results of Isfahani and Moghaddam [7].

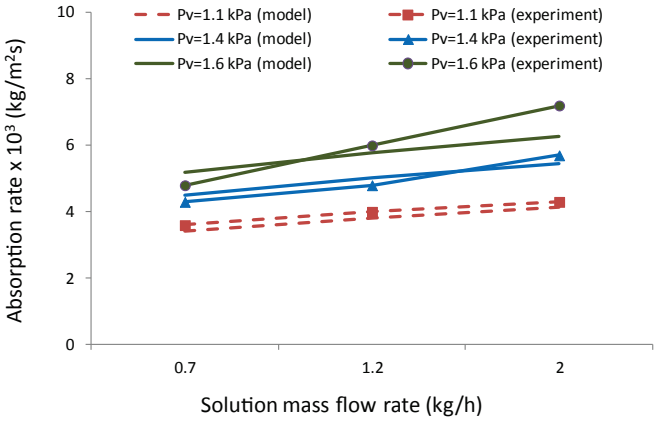

Fig. 6. Absorption rate as a function of the solution mass flow rate and the vapour pressure (P_v). Comparison between model and experimental results of Isfahni and Moghaddam [7].

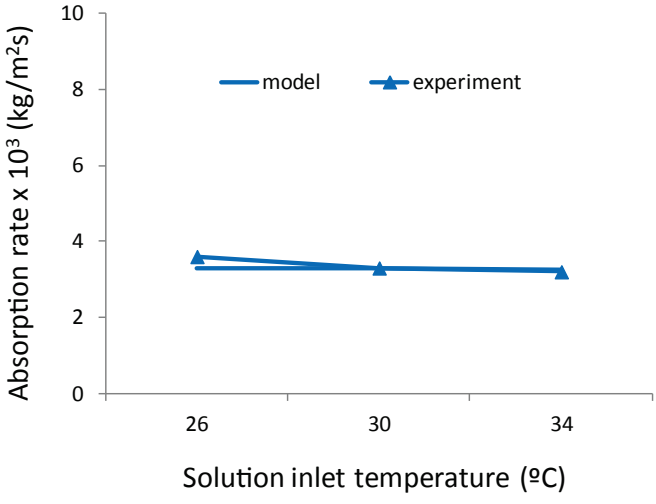

Fig. 7. Absorption rate as a function of the solution inlet temperature. Comparison between model and experimental results of Isfahani and Moghaddam [7].

the increase of the solution mass flow rate tends to increase the mass transfer. As discussed earlier in relation to Fig. 4, a higher vapour pressure contributes to increase the absorption rate.

Fig. 7 shows the effect of the solution inlet temperature on the absorption rate. Temperature increase approaches the solution to its equilibrium state, so the driving force for mass transfer de creases. This effect translates into a slight decrease of the absorp tion rate, as observed in the figure. Both model and experimental data show a similar tendency, and small differences exist between them.

The mean absolute error of the model predictions respect to all experimental data represented in Figs. 4–7 is 8.5%. This low dif ference demonstrates the value of the model to perform a good prediction of the miniaturized membrane based absorber perfor mance. Also, it allows evaluating the influence of individual pa rameters on the absorption rate.

3. Results and discussion

In Fig. 8 the variation of the absorption rate along the channel is represented simultaneously with the solution concentration change. The decrease in LiBr mass fraction describes the water vapour absorption process. At the channel entrance, when higher pressure potential and overall mass transfer coefficient are avail able (Fig. 9), the absorption rate is higher. This value tends to decrease as the solution absorbs the vapour along the channel. Absorption rates of $3.2 \cdot 10^{-3}$ kg/m^{2}s on average are obtained in the channel.

As observed in Fig. 10, major resistance to mass transfer moves from membrane to solution side. In the first 2 cm, absorption is controlled by the membrane resistance. From this point, solution mass transfer limits the absorption process. These results have not been found in the literature of microporous membranes applied to absorption chillers, to our knowledge. This reveals the importance of decreasing the mass transfer resistance of both, membrane and solution, to improve the absorption rate. Membrane resistance is controlled mainly by the maximum pore diameter allowable to avoid aqueous solution penetration into the membrane pores, as discussed by Ali and Schwerdt [9]. One way to reduce the solution mass transfer resistance could be to decrease the solution thick ness, which is corroborated by the heat and mass transfer analogy used in the present model. According to this analogy, solution mass transfer resistance decreases if the aspect ratio of the solution channels rises.

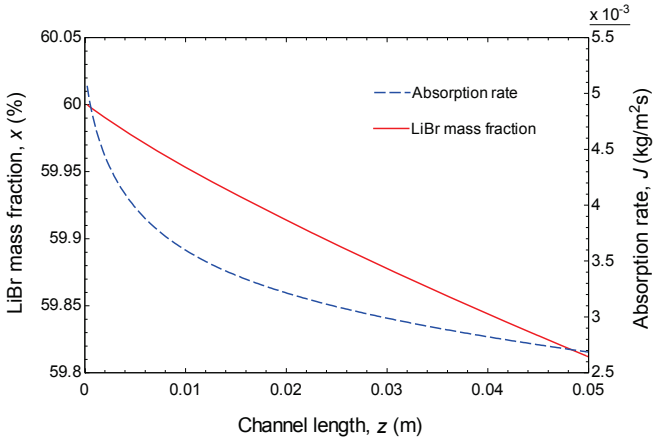

Fig. 8. Evolution of the LiBr mass fraction and absorption rate along the absorption channel.

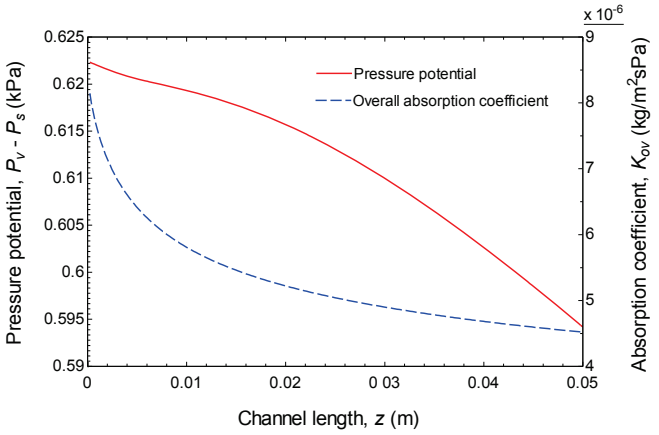

Fig. 9. Evolution of the pressure potential and the overall absorption coefficient along the absorption channel.

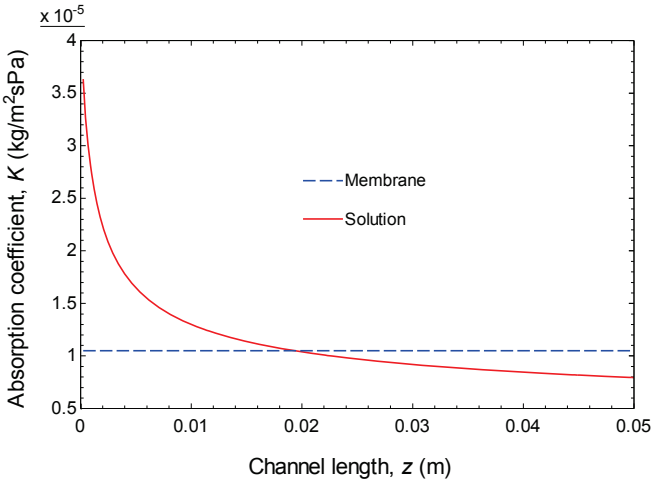

Fig. 10. Evolution of the absorption coefficients along the absorption channel.

Variation of the solution and cooling water temperatures along the absorption channel is shown in Fig. 11. Temperature of the so lution is almost constant initially, due to heat transfer to cooling water, until 2 cm length approximately. From this point, the release of the absorption heat tends to increase both the solution and cooling water temperatures. The first 2 cm of constant solution temperature observed in the figure directly relates to the maximum observed in the absorption parameters represented in Figs. 8–10. It implies that, the lower the solution temperature is, the higher the potential for mass transfer will be.

Fig. 12 represents the evolution of the thermal power stored in the solution and transferred to the cooling water and vapour along the absorption channel. In the first 2 cm of the channel (corre sponding to the solution temperature variation commented in relation to Fig. 11) most of the heat is transferred to the cooling water. After this point, heat is also stored in the solution and, associated to it, is the drop off observed in the absorption rate in Fig. 8. Along the whole absorber, heat is effectively transferred to the cooling water and this heat transfer is always higher than the heat stored in the solution. The contribution of the power trans ferred to the vapour is almost two orders of magnitude smaller.

Very high convection heat transfer coefficients are predicted in the present study for the solution and cooling water flows, as shown in Fig. 13. In these cases the thermal entrance

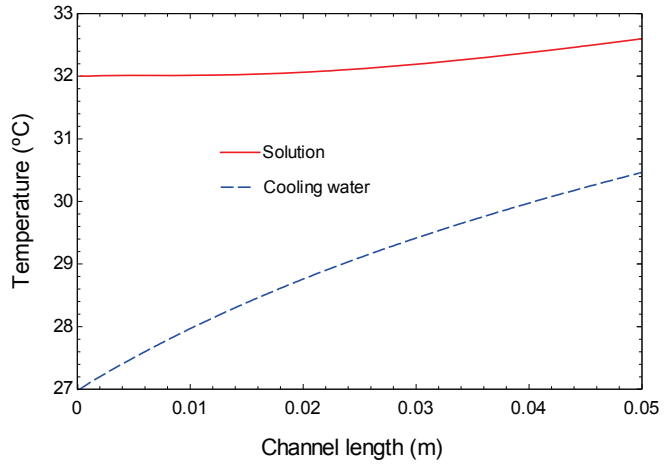

Fig. 11. Evolution of the solution and cooling water temperatures along the absorption channel.

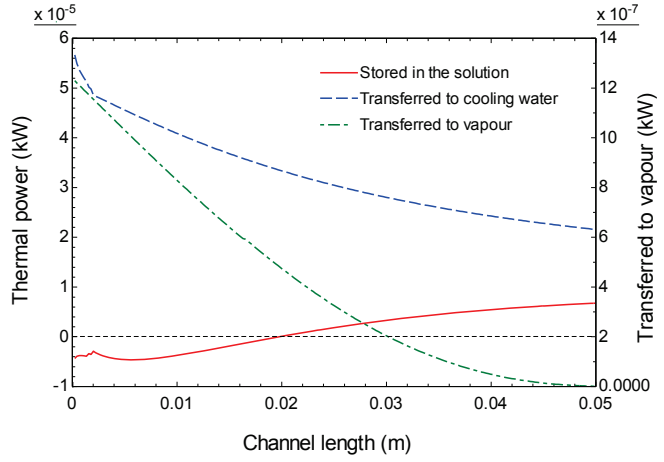

Fig. 12. Evolution of the thermal power transferred to the cooling water and vapour and stored in the solution along the absorption channel.

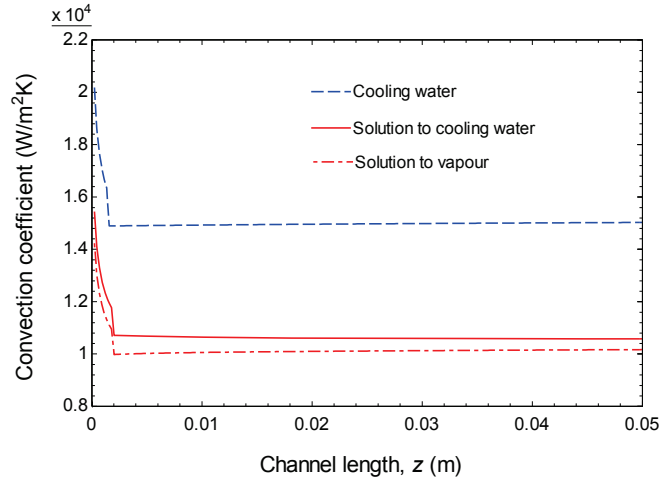

Fig. 13. Evolution of convection coefficients along the absorption channel.

region is about 2 mm in both cases. The strong change observed in the figure for the heat transfer coefficients corre sponds to this point. Additionally, in the fully developed flow region, as the aspect ratio of the channels is constant, the slight increase observed in the convection coefficient of cooling water flow is determined by the change in the thermal con ductivity of the fluid. Regarding the solution flow, the modified heat transfer coefficients (taking into account the effect of mass transfer) are shown. As commented before, convection coefficients for heat transfer to cooling water are higher than those to vapour because absorption takes place in the same direction of heat transfer. In the case of the vapour flow, very low convection coefficients are predicted, between 11.4 and 12 W/m^2K. Along the whole vapour channel the flow is still thermally developing.

Laminar flow is expected to occur in all the cases. In the con ditions evaluated, Reynolds numbers range between 54 and 60, 14–16 and 0.4–27 for the cooling water, solution and vapour, respectively. Velocity of the cooling water and solution are practi cally constant, at 17.2 and 20.1 cm/s respectively. Vapour velocity reduces from 4 m/s to 7 cm/s.

The cooling power of an absorption chiller equipped with the absorber modelled in the present work is represented in Fig. 14 as a function of the channel length. Also, the ratio between this cooling power and the absorber volume is shown. As observed, the ratio suddenly increases with the channel length, reaching its maximum value at 3 mm length. From this point, the ratio slowly decreases. Hence, in order to optimize the absorber size, when designing the absorber it is not recommended to use very long channels, because the increase of the absorber size is higher than the increment ob tained in the cooling power. This is an important conclusion derived from the results of the present model. To the best of our knowledge, it is the first time the ratio between the cooling power and the absorber volume is used to optimize the size of membrane based absorbers.

The maximum value of the ratio between cooling power and absorber volume is 1090 kW/m^3. If the module proposed in Fig. 1 is constructed forming a parallel system, in such a way that the vapour and cooling water channels are shared by the adjacent modules, this ratio can be increased almost twice. This ratio is higher than values found in optimized horizontal falling film ab sorbers using the same solution, as modelled by Jeong and Gar imella [29]. In that study, the ratio reaches maximum values of

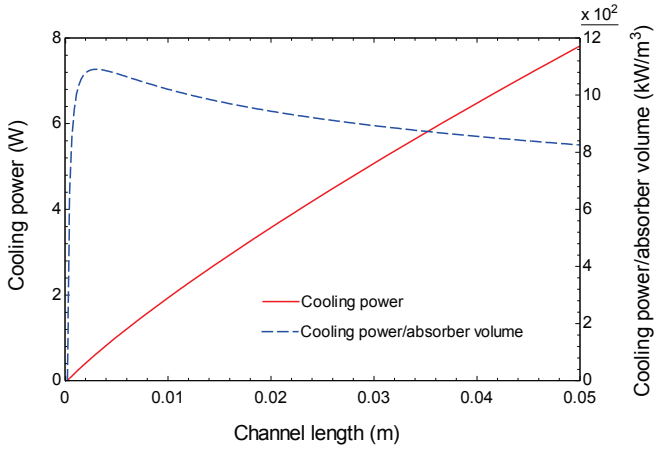

Fig. 14. Evolution of the cooling power and the ratio between the cooling power and the absorber volume along the absorption channel.

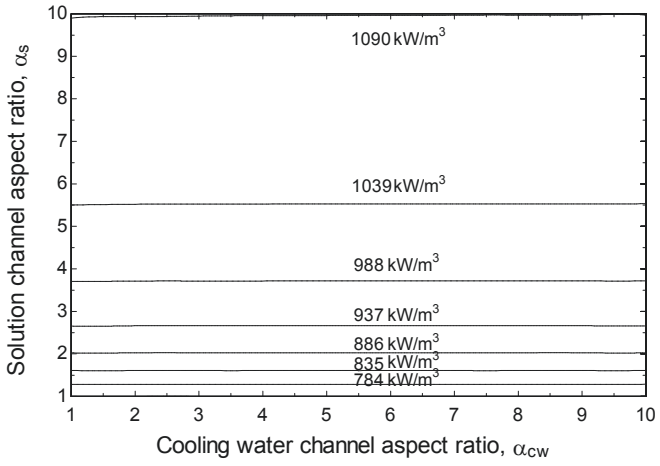

Fig. 15. Ratio between the cooling power and the absorber volume for different aspect ratios of the solution and cooling water channels.

938.3 kW/m^3 for tubes of 3.175 mm diameter, 655.6 kW/m^3 for tubes of 6.35 mm diameter, and 450.7 kW/m^3 for conventional tubes of 15.88 mm diameter. Additionally, wetting of small diameter tubes can be a problem and the cooling capacity can be reduced by about 30% if the one half of the total tube surface is wet (Jeong and Garimella [29]).

The model also allows optimizing the geometry of the absorber channels. Therefore, the influence of the solution and cooling water channels aspect ratios on the performance of the absorber is evaluated in Fig. 15. As it is observed, the aspect ratio of the cooling water channel has a negligible influence on the absorber size. However, the cooling power of the chiller equipped with this absorber notably increases when the solution channels aspect ratio augments. The maximum ratio between this cooling power and the absorber volume is obtained for the maximum value evaluated, α_s 10.

4. Conclusions

In the present paper, a simulation of the heat and mass transfer processes taking place in a miniaturized absorber using membrane technology has been developed. The model has been validated comparing the results with experimental data available in the literature. Novel results have been presented, showing the variation along the channel of: membrane and solution mass transfer co efficients, thermal powers transferred to cooling water and vapour and stored in the solution, convection heat transfer coefficients in the cooling water and solution, cooling power and the ratio be tween the cooling power and the absorber volume. Also, as a novelty, the influence of the aspect ratios of the cooling water and solution channels on the ratio between the cooling power and the absorber volume is given. The following conclusions have been derived:

- The first 2 cm of the absorption channels are the most active for mass transfer. Here the solution is sufficiently cool and is able to efficiently absorb the water vapour. As the solution heats, its absorption potential decreases.
- Mass fraction changes of about 0.2% and average absorption rates of 3.2·10^{-3} kg/m^{2}s are obtained for the conditions simu lated in the present study using an absorber of 5 cm length. Mass transfer coefficients of about 5.2·10^{-6} kg/m^{2}sPa are obtained.
- The simulated absorber has a maximum value of the ratio be tween cooling capacity of the chiller and absorber volume of 1090 kW/m^3. This value is more than twice the one obtained using falling film absorbers of conventional diameter tubes. Additionally, dimensions of the absorber equipped with mem branes can be reduced at about one half of the value here ob tained using a parallel combination of the proposed module.
- In order to maximize the ratio between the cooling capacity of the chiller and the absorber volume, when designing the absorber it is not recommended to use very long channels, because the increase of the absorber size is higher than the increment obtained in the cooling power.
- The aspect ratio of the solution channel has a high influence on the absorber performance. Keeping constant the channel width, when the channel height decreases the absorption rate in creases and the absorber size reduces. This demonstrates the importance of reducing the solution film thickness.
- Comparison between the model predictions and the experi mental results shows a very good agreement. The mean absolute error of the model with respect to experimental data is 8.5%. This demonstrates the applicability of the model to predict the performance of miniaturized membrane based absorbers.
- The influence of geometrical and operational parameters on the absorption rate can be evaluated using the model pre sented. These parameters include the solution channel height, solution and cooling water inlet temperatures, vapour pressure and solution mass flow rate. Therefore, the model can be used to optimize the geometry and operating conditions of the absorber.

Acknowledgements

The financial support of this study by the Ministerio de Econo mía y Competitividad of Spain through the research grant ENE2013 43131 R is greatly appreciated.

References

[1] García-Hernando N, Almendros-Ibanez JA, Ruiz G, de Vega M. On the pressure drop in plate heat exchangers used as desorbers in absorption chillers. Energy Convers Manag 2011;52:1520 5.
[2] Venegas M, Arzoz D, Rodríguez P, Izquierdo M. Heat and mass transfer in $LiNO_3$-NH_3 spray absorption system. Int Commun Heat Mass Transf 2003;30: 805 15.
[3] de Vega M, Almendros-Ibanez JA, Ruiz G. Performance of a LiBr water absorption chiller operating with plate heat exchangers. Energy Convers Manag 2006;47:3393 407.
[4] Chen J, Chang H, Chen S-R. Simulation study of a hybrid absorber-heat exchanger using hollow fiber membrane module for the ammonia-water absorption cycle. Int J Refrig 2006;29:1043 52.
[5] Schaal F, Weimer T, Hasse H. Membrane contactors for absorption refrigeration. Seoul, Korea: International Sorption Heat Pump Conference; 2008.
[6] Ghiasi C, Martí-Calatayud MC, Weimer T, Ziegler F. Ammonia-water absorption heat pumps with membrane absorber. 2009. IIR Conference: Ammonia Refrigeration Technology, Ohrid.
[7] Isfahani RN, Moghaddam S. Absorption characteristics of lithium bromide (LiBr) solution constrained by superhydrophobic nanofibrous structures. Int J Heat Mass Transf 2013;63:82 90.
[8] Isfahani RN, Sampath K, Moghaddam S. Nanofibrous membrane-based absorption refrigeration system. Int J Refrig 2013;36:2297 307.
[9] Ali AHH, Schwerdt P. Characteristics of the membrane utilized in a compact absorber for lithium bromide-water absorption chillers. Int J Refrig 2009;32: 1886 96.
[10] Yu D, Chung J, Moghaddam S. Parametric study of water vapour absorption into a constrained thin film of lithium bromide solution. Int J Heat Mass Transf 2012;55:5687 95.
[11] Bigham S, Yu D, Chugh D, Moghaddam S. Moving beyond the limits of mass transport in liquid absorbent microfilms through the implementation of surface-induced vortices. Energy 2014;65:621 30.
[12] Asfand F, Bourouis M. A review of membrane contactors applied in absorption refrigeration systems. Renew Sustain Energy Rev 2015;45:173 91.
[13] Henning HM. Solar assisted air conditioning of buildings an overview. Appl Therm Eng 2007;27:1734 49.

[14] Ali AHH. Design of a compact absorber with a hydrophobic membrane contactor at the liquid vapor interface for lithium bromide water absorption chillers. Appl Energy 2010;87:1112 21.
[15] Klein SA. Engineering equation solver. Academic Professional, 1992 2014, V9.698-3D. 2014.
[16] Patek J, Klomfar J. A computationally effective formulation of the thermodynamic properties of LiBr-H2O from 273 to 500 K over full composition range. Int J Refrig 2006;29:566 78.
[17] DiGuilio RM, Lee RJ, Jeter SM, Teja AS. Properties of lithium bromide-water solutions at high temperatures and concentrations I thermal conductivity. ASHRAE Trans 1990;RP-527:702 8.
[18] Harr L, Gallagher JS, Kell GS. NBS/NRC steam tables. Hemisphere Publishing Co; 1984.
[19] Electrical Research Association Steam Tables. Thermodynamic properties of water and steam; viscosity of water and steam, thermal conductivity of water and steam. London: Edward Arnold Publishers; 1967.
[20] Chawla SL, Gupta RK. Materials selection for corrosion control. ASM Int 1993: 272.
[21] Redhead PA, Hobson JP, Kornelsen EV. The physical basis of ultrahigh vacuum. Chapman and Hall; 1968.
[22] Mason EA, Malinauskas AP. Gas transport in porous media: the dusty-gas model. Elsevier; 1983.
[23] Iversen SB, Bhatia VK, Dam-Johansen K, Jonsson G. Characterization of microporous membranes for use in membrane contactors. J Membr Sci 1997;130:205 17.
[24] Lee P-S, Garimella SV. Thermally developing flow and heat transfer in rectangular microchannels of different aspect ratios. Int J Heat Mass Transf 2006;49:3060 7.
[25] Shah RK, London AL. Laminar flow forced convection in ducts, in: a source book for compact heat exchanger analytical data. Advances in heat transfer. NewYork: Academic Press; 1978. Suppl. 1.
[26] Mittermaier M, Schulze P, Ziegler F. A numerical model for combined heat and mass transfer in a laminar liquid falling film with simplified hydrodynamics. Int J Heat Mass Transf 2014;70:990 1002.
[27] Taylor R, Krishna R. Multicomponent mass transfer. New York: John Wiley & Sons; 1993.
[28] Martínez L, Rodríguez-Maroto JM. Characterization of membrane distillation modules and analysis of mass flux enhancement by channel spacers. J Membr Sci 2006;274:123 37.
[29] Jeong S, Garimella S. Optimal design of compact horizontal tube LiBr/water absorbers. HVAC&R Res 2005;11:27 44.